Separation and Purification Technology 87 (2012) 120–126

Contents lists available at SciVerse ScienceDirect

Separation and Purification Technology

journal homepage: www.elsevier.com/locate/seppur

A comparison of the CO_2 capture characteristics of zeolites and metal–organic frameworks

Rajamani Krishna *, Jasper M. van Baten

Van 't Hoff Institute for Molecular Sciences, University of Amsterdam, Science Park 904, 1098 XH Amsterdam, The Netherlands

ARTICLE INFO

Article history:
Received 31 August 2011
Received in revised form 19 November 2011
Accepted 22 November 2011
Available online 30 November 2011

Keywords:
CO_2 capture
Pressure swing adsorption
Metal organic frameworks
Zeolites
Selectivities

ABSTRACT

Considerable progress has been made in recent years on the development of novel adsorbents for CO_2 capture. Pressure swing adsorption (PSA), using a packed bed of adsorbents is one of the leading contenders for use in technological applications. The candidate adsorbents are often structured micro-porous materials such as metal organic frameworks (MOFs), zeolitic imidazolate frameworks (ZIFs), and zeolites. The most common method of screening and selecting adsorbents is on the basis of adsorption *selectivity*. Besides adsorption selectivity, the performance, and economics, of a PSA unit is governed by a number of other factors, notably the working *capacity*. The main objective of this study is to investigate the relative importance of selectivity and capacity on PSA performance. Breakthrough characteristics of a packed bed adsorber packed with a number of zeolites (MFI, JBW, AFX, NaX), and MOFs (MgMOF-74, MOF-177, CuBTTri-mmen) were investigated for CO_2 capture from a CO_2/N_2 mixture. These breakthrough calculations demonstrate that high capacities could have a dominant influence on the overall performance of PSA units. Our studies indicate that MgMOF-74 is the best adsorbent for post-combustion CO_2 capture.

1. Introduction

For separation of CO_2 from streams containing CH_4, N_2, and H_2 in pre- or post-combustion processing and natural gas sweetening, adsorptive separations using zeolites, metal organic frameworks (MOFs), and zeolitic imidazolate frameworks (ZIFs) offer energy efficient alternatives to more conventional separation techniques such as amine absorption [1–8]. In particular, with MOFs, a wide variety of strategies can be adopted to enhance the CO_2 uptake; these include appropriate choice of ligand design [9], the introduction of non-framework cations [10], use of exposed metal cation sites [2,3,5,11–13], and incorporation of functional groups within a framework [4,14].

Pressure swing adsorption (PSA) with a fixed bed of adsorbent particles is often the technology of choice. For a given feed composition, and set of operating conditions such as pressure and temperature, the economics of CO_2 capture in PSA units are dictated by several factors [15], of which the primary metric is considered to be the adsorption selectivity, S_{ads}, defined by:

$$S_{ads} = \frac{q_1/q_2}{p_1/p_2}, \tag{1}$$

where the q_i represent the component molar loadings in equilibrium with a bulk fluid phase with partial pressures p_i.

Besides S_{ads}, another important metric that determines the economics of PSA units is the working capacity [2,15,16]. This metric is defined as the difference in the loadings of the component that needs to be preferentially adsorbed, expressed in mol per kg of microporous crystalline material, at the "adsorption" pressure minus the corresponding loading at the "desorption", or purge, pressure. The adsorption pressure could be in the 0.1–10 MPa range, and the desorption pressure could be 0.01–0.1 MPa.

The major objectives of the present communication are twofold. Firstly, we highlight the variety of factors that determine selectivity and capacity metrics of zeolites and MOFs for separation of CO_2/CH_4, CO_2/H_2, and CO_2/N_2 mixtures. Secondly, we underscore the *relative* importance of the selectivity and capacity metrics by performing breakthrough calculations in a fixed bed adsorber under conditions that are representative of post-combustion CO_2 capture. The important message that will be conveyed is that choosing adsorbents purely based on selectivity considerations is not justified; capacity considerations often have dominant, and overriding, effects. The suggested methodology for screening adsorbents must be viewed as a preliminary screening exercise, to be confirmed by breakthrough experiments, and investigations on regenerability aspects. The current study is not intended as a substitute for detailed process design of PSA processes.

2. Adsorption selectivity

For a given separation task, the adsorption selectivity is governed by a wide variety of factors that include pore size and

* Corresponding author. Tel.: +31 20 6270990; fax: +31 20 5255604.
E-mail address: r.krishna@uva.nl (R. Krishna).

1383-5866/$ - see front matter © 2011 Elsevier B.V. All rights reserved.
doi:10.1016/j.seppur.2011.11.031

geometry. There is an extremely wide variation in the values of the surface areas, pore volumes, and characteristic pore dimensions of zeolites and MOFs, as illustrated in the data presented in Fig. 1a and b for a few chosen materials that will be investigated in detail in this article. The characteristic pore dimension is determined by following the method of Delaunay triangulation described in the work by Foster et al. [17]; this corresponds with the *maximum* hard-sphere diameter that can pass through the channels. Of the commonly used zeolites, FAU has the most "open" structure, with a characteristic size (window aperture) of 7.4 Å, a pore volume of 0.33 cm^3/g, and a surface area of 1086 m^2/g. Many important MOFs have significantly higher pore volumes, surface areas, and channel sizes.

The adsorbent with the highest selectivity for a given CO_2 separation duty can selected on the basis of screening of available zeolites and MOFs. The screening can be done on the basis of experiments [2,3,8,18,19], or molecular simulations [6,7,20,21]. For all-silica zeolites, molecular simulations are potent tools because the force fields are considered to be transferable from one zeolite to another, and have been developed for a variety of guest molecules are based on extensive experimental data on pure component isotherms [22–26]. As illustration, Fig. 2 presents data obtained from Configurational-Bias Monte Carlo (CBMC) simulations on the selectivity for CO_2/CH_4, and CO_2/H_2 mixtures as a function of the total gas pressure for a selection of all-silica zeolites: AFX, JBW, BIK, SIV, LOV, LEV, EPI, CHA, MFI, and FAU-Si. The simulations were carried out to a total pressure of 10 MPa in order to be of rel-

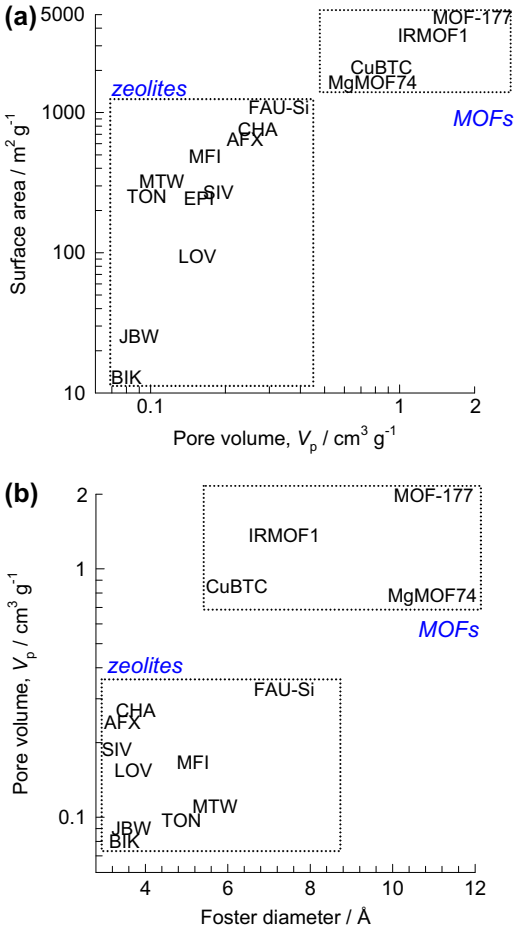

Fig. 1. (a) Data on surface area vs pore volumes, and (b) pore volumes vs characteristic dimensions (Foster diameter [17]) for some representative zeolites and MOFs. The data are obtained using the simulation methodology described in the Supplementary material accompanying this article.

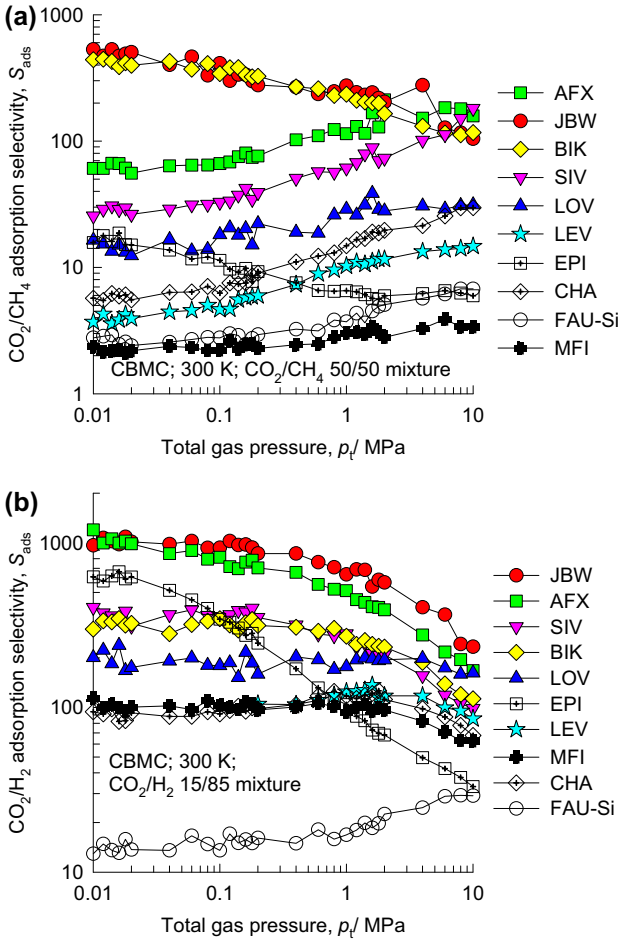

Fig. 2. Adsorption selectivities for (a) CO_2/CH_4, and (b) CO_2/H_2 mixtures at 300 K in a variety of all-silica zeolite structures, obtained from Configurational-Bias Monte Carlo (CBMC) simulations. In (a) the partial fugacities in the gas phase are equal, i.e. $p_1 = p_2$. In (b) the gas phase partial fugacities satisfy $p_1/p_2 = 15/85$. The data plotted here are obtained from the Supplementary material accompanying this article.

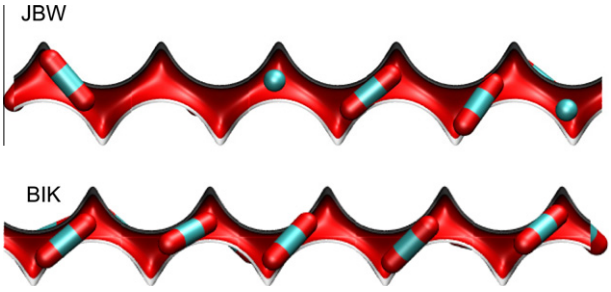

Fig. 3. Snapshot showing the location of CO_2 and CH_4 molecules within the 1D zigzag channels of JBW and BIK. Video animations showing the motion of guest molecules in JBW and BIK are available as Supplementary material.

evance to natural gas and H_2 purification technologies for which pressures as high as 5 MPa are used. The zeolites have been chosen on the basis of the information available in earlier works [7,27,28]. For any mixture, the values of S_{ads} are seen to vary by 2–3 orders of magnitude. It is noteworthy that for JBW, BIK, and AFX, selectivities in the range 100–1000 are obtained for both mixtures. The reasons for the high selectivities can be explained on the basis of snapshots of the adsorbed CO_2 in these three structures. JBW and BIK are both one-dimensional 8-ring channel structures of about 3.7 Å size. The channel topologies are such that CO_2 can nestle nicely in each chan-

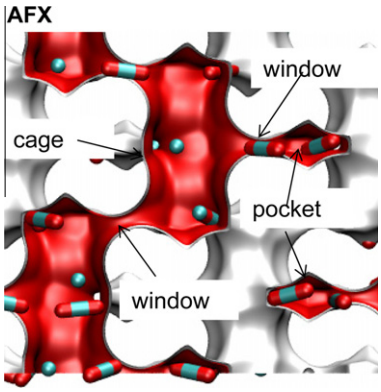

Fig. 4. Pore landscape of AFX, showing the location of CO_2 molecules. Video animations showing the motion of guest molecules in AFX are available as Supplementary material.

nel segment (cf. Fig. 3); these are like "egg-cartons" for CO_2. Interestingly, JBW and BIK have the lowest values of pore volumes and surface areas. The preferential perching of CO_2 at the window regions and within pockets (cf. Fig. 4) accounts for the high selectivities obtained with AFX [7,28,29]. There are no experimental data to confirm the high selectivity expectations for JBW, BIK, and AFX.

Though there are several papers using molecular simulation techniques for screening MOFs [7,21], the available force fields are not as reliable as for all-silica zeolites. To underscore this point, we compare the CBMC simulations of the CO_2 isotherm in MgMOF-74 (also denoted as CPO-27-Mg, or Mg_2(dobdc) with dobdc = (dobdc^{4-} = 1,4-dioxido-2,5-benzenedicarboxylate) at 300 K, with the force field developed by Yazaydin et al. [5], with the experimental data of Dietzel et al. [30]; see Fig. 5a. The experimental data show an inflection at a loading of about 8 mol/kg that corresponds to one molecule of 1 CO_2 per atom of Mg in the framework. We note that for pressures exceeding 0.1 MPa, there is excellent agreement between the CBMC simulations and experiment. However, for pressures below 0.1 MPa, the experimental loadings are significantly higher than the simulated values. The reason for this deviation at pressures below 0.1 MPa can be traced to the fact that the force field implementation of Yazaydin et al. [5] does not explicitly account for orbital interactions and polarization. Such effects are particularly strong in the low pressure region; the influence of polarization is of lesser importance at higher pressures. When the guest species do not have orbital interactions with the Mg atoms, the predictions of the CBMC simulations can be expected to be good. Fig. 5b compares CBMC simulations of the adsorption isotherms for CH_4 at 300 K with the experimental data of Dietzel et al. [30]; the agreement between the two sets is good for the entire pressure range. CBMC simulations of the selectivity of CO_2/CH_4 mixtures are significantly lower, by a factor of five, than those obtained from IAST calculations using fits of experimental isotherm data; see Fig. 5c.

The important conclusion we draw from Fig. 5 is that molecular simulations can lead to pessimistic estimates of selectivity for MOFs that have affinity for CO_2. For MOFs structures decorated with amine functional groups [4,14], appropriate force fields are unavailable. For a fair comparison of MOFs with all-silica zeolites, therefore, we need to rely on IAST calculations of S_{ads} based on pure component isotherm fits of experimental data.

3. Selectivity vs capacity considerations in post-combustion CO_2 capture

The selectivity and capacity metrics do not go hand-in-hand. To demonstrate this, let us consider the separation of CO_2/N_2 mixtures

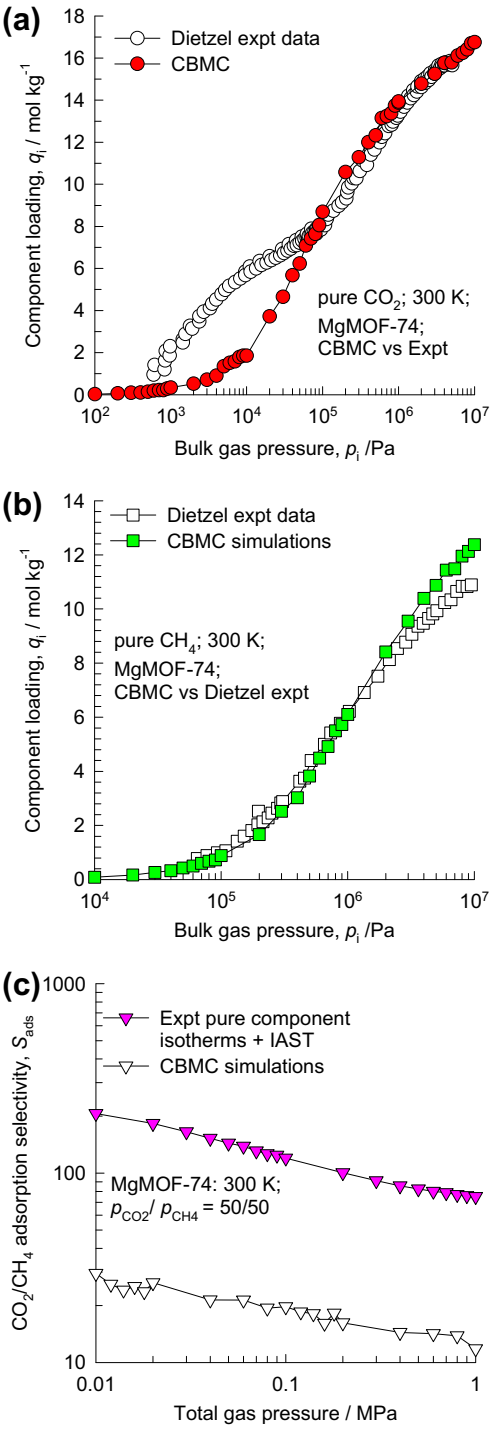

Fig. 5. Comparison of the CBMC simulations of the pure component adsorption isotherms for (a) CO_2, and (b) CH_4 in MgMOF-74 at 300 K with experimental data of Dietzel et al. [30]. (c) Comparison of CBMC simulations of adsorption selectivity of CO_2/CH_4 mixture in MgMOF-74 at 300 K with IAST calculations using pure component isotherm fits of experimental isotherm data [30].

with the composition 15% CO_2 and 85% N_2 that is relevant in post-combustion processing. Experimental and theoretical studies have indicated that MgMOF-74 is a suitable adsorbent for this separation [3,7,18,31]. For CuBTTri functionalized with *N*,*N*′-dimethylethylenediamine (this structure is denoted here as mmen-CuBTTri), the more recent work of McDonald et al. [4] claims that "the selectivity observed at 25 °C is the highest value yet reported for a metal–organic framework". This claim is indeed substantiated by

our IAST calculations of S_{ads} at 300 K presented in the Fig. 6a for MgMOF-74, and mmen-CuBTTri. Also presented in Fig. 6a are data on S_{ads} for MOF-177, four different all-silica zeolites (JBW, AFX, FAU-Si, and MFI) and NaX. The electrostatic interactions of CO_2 with the Na^+ cations lead to significantly higher values of S_{ads} of NaX when compared to FAU-Si [6,7,32]. Remarkably the highest selectivity is obtained with JBW over the entire range of pressures. At a total system pressure p_t = 0.1 MPa, typical of post-combustion capture conditions, the hierarchy of adsorption selectivities is found to be JBW > mmen-CuBTTri > AFX ≈ MgMOF-74 > NaX ≫ MFI > FAU-Si > MOF-177.

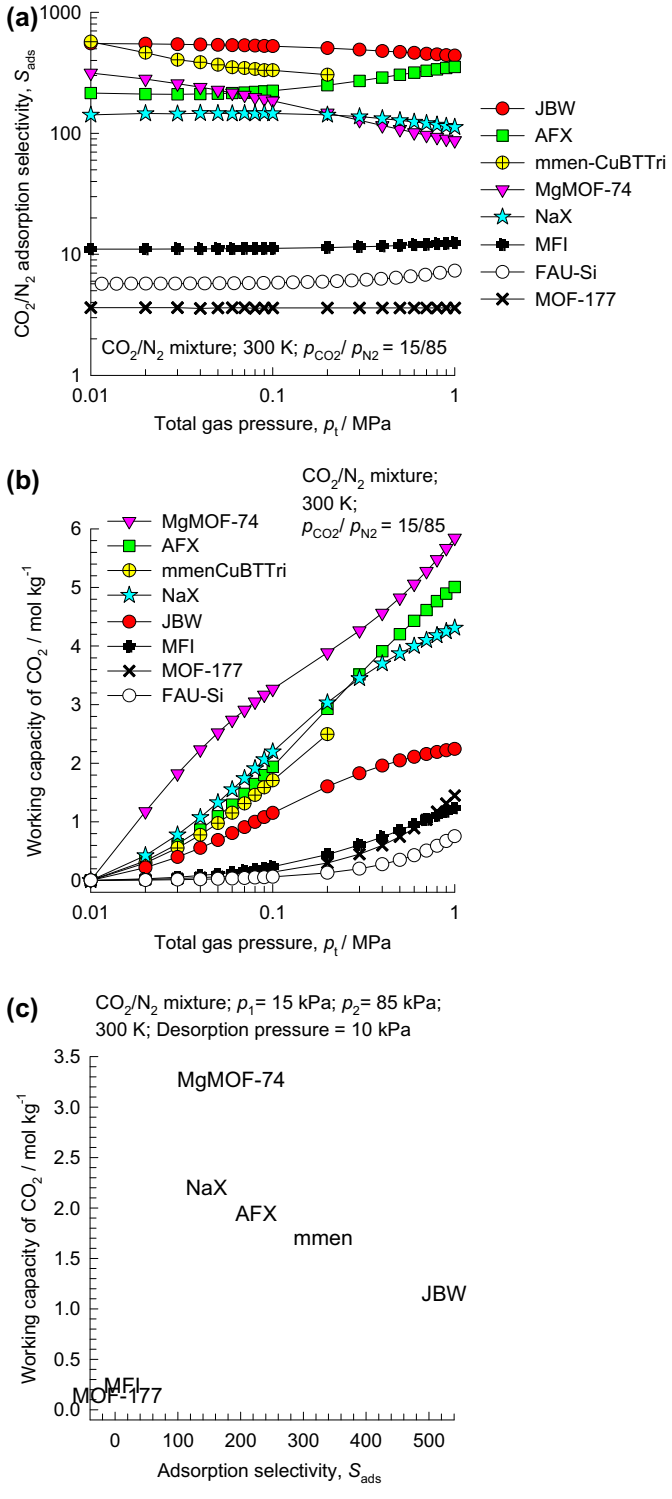

Fig. 6. (a) Adsorption selectivities, S_{ads}, for CO_2/N_2 mixtures (15% CO_2, 85% N_2) at 300 K for zeolites (MFI, JBW, AFX, NaX, FAU-Si), and MOFs (MgMOF-74, MOF-177, CuBTTri-mmen) as a function of the total gas phase pressure. (b) Working capacity of CO_2 for adsorption from the 15/85 CO_2/N_2 mixtures; the desorption pressure is chosen to be 10 kPa. (c) Plot of working capacity vs S_{ads} for a total pressure of 100 kPa. The data for all-silica JBW, AFX, and MFI are obtained from molecular simulations. For all other structures the data are based on IAST calculations using pure component isotherm fits. The parameter values for pure component isotherm fits are provided in the Supplementary material accompanying this article.

The adsorbent that has the highest S_{ads} value, JBW, has the smallest values of pore volume, and surface area; see Fig. 1. We should therefore expect a significantly lower capacity of JBW to adsorb CO_2. This is confirmed in the data presented in Fig. 6b for the working capacity for CO_2 adsorption for the binary mixture (15% CO_2 and 85% N_2) by the different materials. The working capacity is defined as the component loading at the adsorption pressure minus the loading at a desorption pressure of 10 kPa. At p_t = 100 kPa, the hierarchy of working capacity values is MgMOF-74 ≫ NaX > AFX > mmen-CuBTTri > JBW > MFI ≈ FAU-Si ≈ MOF-177. Due to the introduction of *N,N′*-dimethylethylenediamine functional groups into the framework, the pore volume of mmen-CuBTTri equals 0.363 cm^3/g which is significantly lower than value of 0.573 cm^3/g for MgMOF-74; this lower pore volume explains the significantly working capacity of CO_2 for mmen-CuBTTri. For a total pressure p_t = 100 kPa, a plot of the working capacity vs S_{ads} summarizes the dilemma in using the two conventional metrics for screening materials. Fig. 6c shows that JBW has the highest S_{ads} but MgMOF-74 has the highest working capacity.

In order to resolve the dilemma on how to weigh the selectivity and capacity characteristics, we need to investigate the relative performances under conditions that are relevant to realistic PSA operations. For this purpose we determined the breakthrough characteristics in a fixed bed adsorber; see schematic in Fig. 7. Assuming plug flow of $CO_2(1)/N_2(2)$ gas mixture through a fixed bed maintained under isothermal conditions and negligible pressure drop, the partial pressures in the gas phase at any position and instant of time are obtained by solving the following set of partial differential equations for each of the species i in the gas mixture.

$$\frac{1}{RT}\varepsilon\frac{\partial p_i}{\partial t} = -\frac{1}{RT}\frac{\partial (up_i)}{\partial z} - (1-\varepsilon)\rho\frac{\partial q_i}{\partial t}; \quad i = 1,2 \tag{2}$$

In Eq. (2), t is the time, z is the distance along the adsorber, ρ is the framework density, ε is the bed voidage, and u is the superficial gas velocity. The molar loadings within the crystallites of the species i, q_i, at any position z, and time t is determined from IAST calculations. Details of the numerical procedures used are available in earlier works [33,34]. Diffusional aspects are not considered in the breakthrough simulations reported here; such aspects need to be considered at a later process design stage.

As illustration, the molar concentrations of the gas phase exiting the adsorber packed with MgMOF-74, with feed of $CO_2(1)/N_2(2)$ mixtures at p_1 = 15 kPa, p_2 = 85 kPa, are shown in Fig. 7. The x-axis is a *dimensionless* time, τ, obtained by dividing the actual time, t, by the contact time between the gas and the crystallites, $\varepsilon L/u$. For a given adsorbent, under chosen operating conditions, the breakthrough characteristics are uniquely defined by τ, allowing the results to be presented here to be equally applicable to laboratory scale equipment as well as to industrial scale adsorbers.

The breakthrough of N_2 occurs earliest, practically near the start of the operations. The breakthrough of CO_2 occurs significantly later. For different zeolites and MOFs, Fig. 8 presents a comparison of the breakthrough curves showing the mole% CO_2 in the outlet gas mixture. For a specified purity of CO_2 in the outlet gas, arbitrarily chosen as 0.05 mol% CO_2, the hierarchy of the dimensionless breakthrough times, τ_{break}, were determined as follows: MgMOF-74 ≫ NaX > AFX > JBW ≈ mmen-CuBTTri ≫ MFI ≫ MOF-177. Higher val-

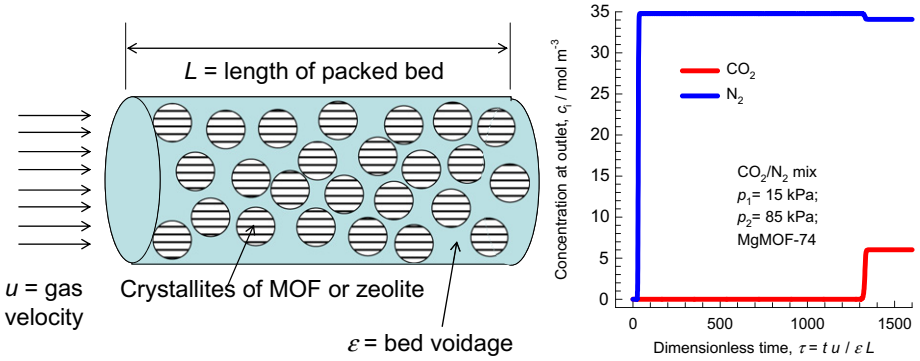

Fig. 7. Schematic of packed bed adsorber, along with data on the breakthrough characteristics of an adsorber packed with MgMOF-74 crystallites with feed of $CO_2(1)/N_2(2)$ mixture with p_1 = 15 kPa, p_2 = 85 kPa. Specifically, the calculations presented here were performed taking the following parameter values: L = 0.1 m; ε = 0.4; u = 0.04 m/s (at inlet).

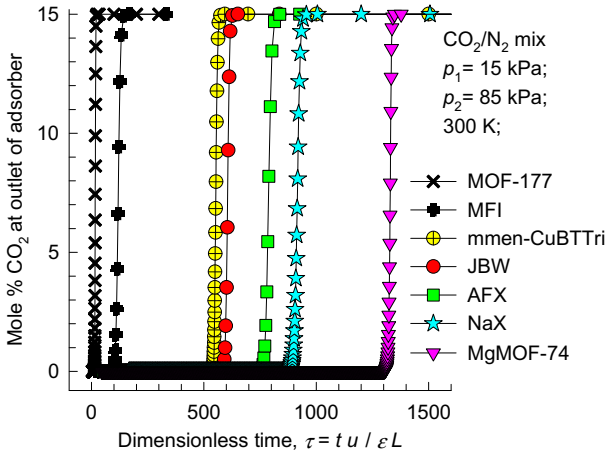

Fig. 8. Breakthrough curves showing the mole% CO_2 in the outlet of packed bed adsorber with step-input of 15/85 CO_2/N_2 mixture at a total pressure of 0.1 MPa and 300 K. Specifically, the calculations presented here were performed taking the following parameter values: L = 0.1 m; ε = 0.4; u = 0.04 m/s (at inlet). Video animations of the traveling concentration fronts traversing the packed bed are uploaded as Supplementary material accompanying this article.

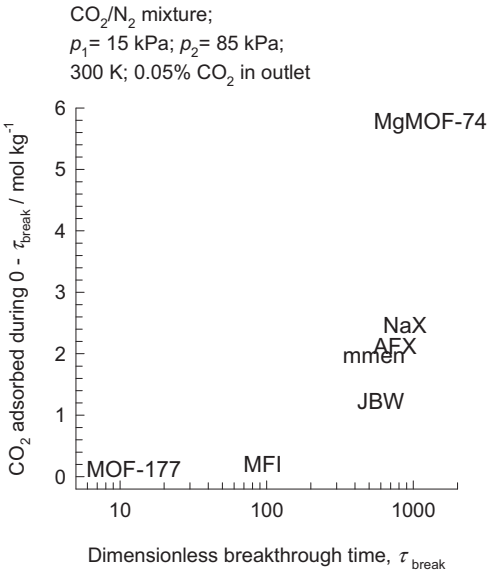

Fig. 9. Plot of the number of moles of CO_2 adsorbed per kg of adsorbent material during the time interval 0–τ_{break} against the breakthrough time τ_{break} for packed bed adsorber with step-input of a 15/85 CO_2/N_2 mixture at 300 K and total pressures of 0.1 MPa. The breakthrough times, τ_{break}, correspond to those when the outlet gas contains 0.05 mol% CO_2.

ues of τ_{break} are desirable because longer times will be available for uptake of CO_2 before the bed needs to be regenerated. The dimensionless breakthrough times reflect a *combination* of the two metrics: S_{ads}, and working capacity. JBW zeolite that has the highest value of S_{ads} (Fig. 6a) has severe capacity limitations (Fig. 6a) and consequently its value of τ_{break} is significantly lower than that of MgMOF-74. When comparing JBW and mmen-CuBTTri we note that S_{ads} for JBW is higher than for mmen-CuBTTri, whereas the latter has a higher working capacity. The net outcome is that the values of τ_{break} for JBW and mmen-CuBTTri are nearly the same.

The economics of a PSA unit for post-combustion CO_2 capture will be dictated primarily by the amount of CO_2 uptake during the adsorption cycle, i.e. during the time interval 0–τ_{break}; this amount can be determined from a material balance. Fig. 9 presents a plot of the number of moles of CO_2 adsorbed per kg of adsorbent material during the time interval 0–τ_{break} against the breakthrough time τ_{break}. From this plot we note that MgMOF-74 has the ability to adsorb more than twice the amount compared to any other material. The significantly higher working capacity of MgMOF-74 (cf. Fig. 6b), outweighs the fact that its selectivity is not the highest amongst the chosen materials (cf. Fig. 6a).

A further point to note is that the hierarchy of materials that emerge from our recommended screening procedure, presented in Fig. 9 is practically the same as that arrived at using working capacity as the metric (cf. Fig. 6c). There are however some additional insights that breakthrough calculations provide. This is illustrated by a comparison of MgMOF-74 with NaX, the two best materials emerging from our screening exercise. MgMOF-74 has both higher selectivity and higher working capacity than NaX. A combination of these two factors results in the fact that MgMOF-74 can adsorb twice as much as NaX in the adsorption cycle; see Fig. 9. Purely on the basis of the working capacity, we find that MgMOF-74 has only a 50% advantage when compared to NaX.

4. Conclusions

By performing transient breakthrough simulations of $CO_2(1)/N_2(2)$ mixtures in a packed bed adsorber, we have examined the variety of factors that influence the performance of a PSA unit. The following major conclusions emerge from our investigations.

(1) Both metrics, adsorption selectivity, S_{ads}, and the CO_2 working capacity, influence the CO_2 capture capacity in a PSA unit.

(2) The dimensionless breakthrough time, τ_{break}, reflects the right combination of the selectivity and capacity metrics that is a proper measure of the performance of PSA units. A high value of τ_{break} is desirable in practice because it reduces the frequency of required regeneration.
(3) The amount of component adsorbed during the interval 0–τ_{break} is a measure of the productivity of the PSA unit.
(4) For post-combustion capture, MgMOF-74 is the ideal choice for use as adsorbent; its CO_2 capture capacity is more than twice that of other material investigated here.

Based on the results of our preliminary screening study, the next step would be to seek experimental confirmation of the viability of MgMOF-74 in practice by also examining intraparticle diffusion, stability, and regeneration aspects. This may be followed up by process design studies on cyclical PSA operations.

5. Notation

L	length of packed bed adsorber, m
p_i	partial pressure of species i in mixture, Pa
p_t	total system pressure, Pa
q_i	component molar loading of species i, mol kg^{-1}
R	gas constant, 8.314 J mol^{-1} K^{-1}
S_{ads}	adsorption selectivity, dimensionless
t	time, s
T	absolute temperature, K
u	superficial gas velocity entering the packed bed, m s^{-1}
V_p	accessible pore volume, m^3 kg^{-1}
z	distance along the adsorber, m

Greek letters

ε	voidage of packed bed, dimensionless
ρ	framework density, kg m^{-3}
τ	time, dimensionless
τ_{break}	breakthrough time, dimensionless

Subscripts

i	referring to component i
t	referring to total mixture

Acknowledgments

This material is based upon work supported as part of the Center for Gas Separations Relevant to Clean Energy Technologies, an Energy Frontier Research Center funded by the US Department of Energy, Office of Science, Office of Basic Energy Sciences under Award Number DE-SC0001015.

Appendix A. Supplementary data

This material includes a document containing: (a) The pore landscapes, and structural details of all-silica zeolites, (b) molecular simulation methodology, and detailed results of adsorption isotherms, (c) pure component isotherm fit parameters used. Also uploaded as Supplementary Material are video animations of breakthrough characteristics, and motion of guest molecules within AFX, JBW, and BIK. Supplementary data associated with this article can be found, in the online version, at doi:10.1016/j.seppur.2011.11.031.

References

[1] D.M. D'Alessandro, B. Smit, J.R. Long, Carbon dioxide capture: current trends and prospects for new materials, Angew. Chem. Int. Ed. 49 (2010) 6058–6082.
[2] Z.R. Herm, J.A. Swisher, B. Smit, R. Krishna, J.R. Long, Metal–organic frameworks as adsorbents for hydrogen purification and pre-combustion carbon dioxide capture, J. Am. Chem. Soc. 133 (2011) 5664–5667.
[3] J.A. Mason, K. Sumida, Z.R. Herm, R. Krishna, J.R. Long, Evaluating metal–organic frameworks for post-combustion carbon dioxide capture via temperature swing adsorption, Energy Environ. Sci. 3 (2011) 3030–3040.
[4] T.M. McDonald, D.M. D'Alessandro, R. Krishna, J.R. Long, Enhanced carbon dioxide capture upon incorporation of *N,N′*-dimethylethylenediamine in the metal–organic framework CuBTTri, Chem. Sci. 2 (2011) 2022–2028.
[5] A.Ö. Yazaydın, R.Q. Snurr, T.H. Park, K. Koh, J. Liu, M.D. LeVan, A.I. Benin, P. Jakubczak, M. Lanuza, D.B. Galloway, J.J. Low, R.R. Willis, Screening of metal–organic frameworks for carbon dioxide capture from flue gas using a combined experimental and modeling approach, J. Am. Chem. Soc. 131 (2009) 18198–18199.
[6] R. Krishna, J.M. van Baten, In silico screening of zeolite membranes for CO_2 capture, J. Membr. Sci. 360 (2010) 323–333.
[7] R. Krishna, J.M. van Baten, In silico screening of metal–organic frameworks in separation applications, Phys. Chem. Chem. Phys. 13 (2011) 10593–10616.
[8] M. Palomino, A. Corma, F. Rey, New insights on CO_2–methane separation using LTA zeolites with different Si/Al ratios and a first comparison with MOFs, Langmuir 26 (2010) 1910–1917.
[9] D. Zhao, D.J. Timmons, D. Yuan, H. Zhou, Tuning the topology and functionality of metal–organic frameworks by ligand design, Acc. Chem. Res. 44 (2011) 123–133.
[10] J. An, N.L. Rosi, Tuning MOF CO_2 adsorption properties via cation exchange, J. Am. Chem. Soc. 132 (2010) 5578–5579.
[11] D. Britt, H. Furukawa, B. Wang, T.G. Glover, O.M. Yaghi, Highly efficient separation of carbon dioxide by a metal–organic framework replete with open metal sites, Proc. Natl. Acad. Sci. USA 106 (2009) 20637–20640.
[12] E.D. Bloch, L. Murray, W.L. Queen, S. Chavan, S.N. Maximoff, J.P. Bigi, R. Krishna, V.K. Peterson, F. Grandjean, G.J. Long, B. Smit, S. Bordiga, C.M. Brown, J.R. Long, Selective binding of O_2 over N_2 in a redox-active metal–organic framework with open iron(II) coordination sites, J. Am. Chem. Soc. 133 (2011) 14814–14822.
[13] Z.R. Herm, R. Krishna, J.R. Long, CO_2/CH_4, CH_4/H_2 and $CO_2/CH_4/H_2$ separations at high pressures using Mg2(dobdc), Microporous Mesoporous Mater. (2012). (<http://dx.doi.org/10.1016/j.micmat.2011.09.004>).
[14] S. Couck, J.F.M. Denayer, G.V. Baron, T. Rémy, J. Gascon, F. Kapteijn, An amine-functionalized MIL-53 metal–organic framework with large separation power for CO_2 and CH_4, J. Am. Chem. Soc. 131 (2009) 6326–6327.
[15] M.T. Ho, G.W. Allinson, D.E. Wiley, Reducing the cost of CO_2 capture from flue gases using pressure swing adsorption, Ind. Eng. Chem. Res. 47 (2008) 4883–4890.
[16] L. Hamon, E. Jolimaître, G. Pirngruber, CO_2 and CH_4 Separation by adsorption using Cu-BTC metal–organic framework, Ind. Eng. Chem. Res. 49 (2010) 7497–7503.
[17] M.D. Foster, I. Rivin, M.M.J. Treacy, O.D. Friedrichs, A geometric solution to the largest-free-sphere problem in zeolite frameworks, Microporous Mesoporous Mater. 90 (2006) 32–38.
[18] J.M. Simmons, H. Wu, W. Zhou, T. Yildirim, Carbon capture in metal–organic frameworks—a comparative study, Energy Environ. Sci. 4 (2011) 2177–2185.
[19] Z. Bao, L. Yu, Q. Ren, X. Lu, S. Deng, Adsorption of CO_2 and CH_4 on a magnesium-based metal organic framework, J. Colloid Interface Sci. 353 (2011) 549–556.
[20] R. Krishna, J.M. van Baten, Using molecular simulations for screening of zeolites for separation of CO_2/CH_4 mixtures, Chem. Eng. J. 133 (2007) 121–131.
[21] R. Krishna, Describing the diffusion of guest molecules inside porous structures, J. Phys. Chem. C 113 (2009) 19756–19781.
[22] T.J.H. Vlugt, R. Krishna, B. Smit, Molecular simulations of adsorption isotherms for linear and branched alkanes and their mixtures in silicalite, J. Phys. Chem. B 103 (1999) 1102–1118.
[23] S. Calero, D. Dubbeldam, R. Krishna, B. Smit, T.J.H. Vlugt, J.F.M. Denayer, J.A. Martens, T.L.M. Maesen, Understanding the role of sodium during adsorption. A force field for alkanes in sodium exchanged faujasites, J. Am. Chem. Soc. 126 (2004) 11377–11386.
[24] D. Dubbeldam, S. Calero, T.J.H. Vlugt, R. Krishna, T.L.M. Maesen, B. Smit, United atom forcefield for alkanes in nanoporous materials, J. Phys. Chem. B 108 (2004) 12301–12313.
[25] E. García-Pérez, J.B. Parra, C.O. Ania, A. García-Sánchez, J.M. Van Baten, R. Krishna, D. Dubbeldam, S. Calero, A computational study of CO_2, N_2 and CH_4 adsorption in zeolites, Adsorption 13 (2007) 469–476.
[26] A. García-Sánchez, C.O. Ania, J.B. Parra, D. Dubbeldam, T.J.H. Vlugt, R. Krishna, S. Calero, Development of a transferable force field for carbon dioxide adsorption in zeolites, J. Phys. Chem. C 113 (2009) 8814–8820.
[27] A. Bhown, M. Haranczyk, S. Kaye, J.R. Long, E. Masanet, J. Reimer, B. Smit, High-Throughput Discovery of Robust Metal–Organic Frameworks for Carbon Dioxide Capture, University of California, Berkeley, <http://2011showcase.lbl.gov/presentations/CarbonCapture_Smit.pdf>, 2011.
[28] R. Krishna, J.M. van Baten, Investigating cluster formation in adsorption of CO_2, CH_4, and Ar in zeolites and metal organic frameworks at sub-critical temperatures, Langmuir 26 (2010) 3981–3992.
[29] R. Krishna, J.M. van Baten, Segregation effects in adsorption of CO_2 containing mixtures and their consequences for separation selectivities in cage-type zeolites, Sep. Purif. Technol. 61 (2008) 414–423.
[30] P.D.C. Dietzel, V. Besikiotis, R. Blom, Application of metal–organic frameworks with coordinatively unsaturated metal sites in storage and separation of methane and carbon dioxide, J. Mater. Chem. 19 (2009) 7362–7370.

[31] R. Krishna, J.M. van Baten, Investigating the potential of MgMOF-74 membranes for CO_2 capture, J. Membr. Sci. 377 (2011) 249–260.
[32] Y. Belmabkhout, G. Pirngruber, E. Jolimaitre, A. Methivier, A complete experimental approach for synthesis gas separation studies using static gravimetric and column breakthrough experiments, Adsorption 13 (2007) 341–349.
[33] R. Krishna, R. Baur, Modelling issues in zeolite based separation processes, Sep. Purif. Technol. 33 (2003) 213–254.
[34] R. Krishna, J.R. Long, Screening metal–organic frameworks by analysis of transient breakthrough of gas mixtures in a fixed bed adsorber, J. Phys. Chem. C 115 (2011) 12941–12950.